Fuel Cell Performance Implications of Membrane Electrode Assembly Fabrication with Platinum-Nickel Nanowire Catalysts

Scott A. Mauger,[1,=,*] K. C. Neyerlin,[1,=,*] Shaun M. Alia,[1,*] Chilan Ngo,[2,*] Siddharth Komini Babu,[3,a] Katherine E. Hurst,[1] Svitlana Pylypenko,[2,*] Shawn Litster,[3,*] and Bryan S. Pivovar[1,*,z]

[1]*Chemistry and Nanoscience Center, National Renewable Energy Laboratory, Golden, Colorado 80401, USA*
[2]*Department of Chemistry, Colorado School of Mines, Golden, Colorado 80401, USA*
[3]*Department of Mechanical Engineering, Carnegie Mellon University, Pittsburgh, Pennsylvania 15213, USA*

Platinum-nickel nanowire (PtNiNW) catalysts have shown exceptionally high oxygen reduction mass activity in rotating disk electrode measurements. However, the ability to successfully incorporate PtNiNWs into high performance membrane electrode assemblies (MEAs) has been challenging due to their size, shape, density, dispersion characteristics, and corrosion-susceptible nickel core. We have investigated the impact of specific processing steps and electrode composition on observed fuel cell performance and electrochemical properties in order to optimize performance. We have found that nickel ion contamination is a major concern for PtNiNWs that can be addressed through ion exchange in fabricated/tested MEAs or by acid leaching of catalyst materials prior to MEA incorporation, with the latter being the more successful method. Additionally, decreased ionomer incorporation has led to the highest performance demonstrating 238 mA/mg$_{Pt}$ (0.9 V IR-free) for PtNiNWs (pre-leached to 80 wt% Pt) with 9 wt% ionomer incorporation.

 [DOI: 10.1149/2.1061803jes]

Manuscript submitted December 1, 2017; revised manuscript received February 9, 2018. Published March 13, 2018.

Platinum (and Pt alloy) nanoparticles on carbon supports (Pt/C) are the standard catalysts for polymer electrolyte fuel cells (PEMFCs). They are the basis for the thousands of fuel cell vehicles on the road today as well as tens of thousands of stationary polymer electrolyte fuel cell power systems. The performance of membrane electrode assemblies (MEAs) based on Pt/C has been optimized over multiple decades through tuning several parameters including carbon type, Pt to carbon loading, ionomer content/type, ink solvent composition, and coating/drying parameters.[1–6] The implementation of unsupported metal catalysts in PEMFCs has seen much less investigation, and the application of non-Pt/C catalysts often falls back on the processes and compositions that have been optimized for Pt/C. For materials, like the nanowires presented here, it should not come as a surprise that dramatic differences in size/structure and properties (density, dispersability, magnetism, surface conductivity, ionomer interactions) significantly impact electrode performance and there is a need to investigate alternate, optimized fabrication compositions and approaches.

To date, the motivation for the development and application of extended surface electrocatalysts in fuel cells has come largely from the promising work of 3M's nanostructured thin film (NSTF) materials.[7,8] These materials started as Pt thin films, but over the last several years have shifted to PtNi alloys, with much effort devoted to examining the sensitivity of activity to the alloy's composition.[9,10] 3M's NSTF is unique in that it is fabricated on a substrate and hot pressed directly into the membrane to form a MEA. Poly/single crystal studies of inherent catalytic activity and durability of flat metal surfaces further show significant benefits over nanoparticle catalysts consistent with findings of NSTF.[11–13] The advantages of extended surface catalyst over supported nanoparticle catalysts are still a matter of some debate, but have been attributed to a number of different factors, including the number of low coordinated sites (leading to higher specific activity and durability) and surface-enhanced proton conduction (which aids in ion accessibility and can reduce ionomer adsorption losses in activity).[14–20] Extended surface catalysts have also demonstrated durability benefits in the Pt sintering (0.6–0.9 V) and carbon corrosion (> 1.0 V) regimes, avoiding supports and Pt-carbon point contacts which can accelerate carbon oxidation.[13] Metal surfaces also allow for ionomer-free proton conduction,[21] suggesting that extended-surface catalysts may be able to attain a lower oxygen transport resistance at high current density, allowing for a higher performance at rated power.

Pt–alloys are the state-of-the-art materials for high activity oxygen-reduction catalysts. Incorporation of transition metals, particularly cobalt and nickel, into the Pt lattice, is the primary strategy to improve the activity per Pt site. This approach has been the focus of numerous publications, which have successfully demonstrated enhanced mass and specific activity on a laboratory production scale with subsequent testing in rotating disk electrode (RDE) experiments[22–29] and in MEAs.[30–33] However, alloy catalysts add additional complexities. Specifically, the alloys are susceptible to transition metal dissolution, which can decrease catalyst activity and increase membrane resistance, as metal ions displace protons in the ionomer.[34–36] Also, the activity of these catalysts is highly dependent on the ratio of alloy components. With 3M's NSTF, there have been many studies related not only to the composition of the alloy but also the location of the components within the NSTF whiskers.[9,10] Similar to what we have found in the course of developing our PtNiNW catalyst, the activity is also influenced by additional annealing treatments of the material following synthesis.[37,38]

The PtNiNW materials used as the basis for this work have demonstrated exceptionally high mass activity and electrochemical surface area (ECA) in rotating disc electrode (RDE) studies of inherent catalytic properties.[37,39] We commonly refer to these catalyst structures as nanowires, although on many occasions the transition metal core has been removed and they could alternatively be referred to as nanotubes. The nanowires we have investigated generally are up to 10's of microns in length (as-synthesized) with diameters typically between 100–300 nm. The materials used in fuel cell tests fall short of our previously reported performance of these materials because the performance of galvanically displaced materials generally scales poorly at large batch sizes (needed in MEA fabrication), due to a combination of higher concentration (less water to uniformly disperse particles) and decreased temperature control during displacement (oil bath not scaled).[40] Optimizing the scale up, processing, and integration of electrocatalysts that have shown promise for facilitating the oxygen reduction reaction (ORR) is non-trivial and, as stated in a recent publication by Kongkanand and Mathias,[41] must be commensurate with the development of the electrocatalyst itself. Few laboratories outside of commercial suppliers have been able to translate the performance of

=These authors contributed equally to this work.
*Electrochemical Society Member.
[a]Present address: Materials Physics and Applications, Los Alamos National Laboratory, Los Alamos, New Mexico 87545, USA.
[z]E-mail: Bryan.Pivovar@nrel.gov

small-batch synthesis catalysts (<100 mg) in RDE to large-batch synthesis catalysts (100 s mg) in MEAs or RDE. Thus, in parallel to our MEA integration efforts we are also researching scalable production methods.[42]

Processing and integration is complex due to the unique nature of these PtNiNWs. Due to their size, lack of support, and potential for surface assisted proton conduction, the optimal ionomer to catalyst ratio for these materials remains unclear. Understanding the integration of PtNiNW electrocatalysts into fuel cell catalyst layers is crucial to realizing the tremendous potential these materials have demonstrated for ORR. Additionally, we have observed that potential cycling of these materials results in loss of the Ni metal core. Thus, from an MEA standpoint, it is not clear what sort of ex situ processing, if any, may be required to maximize performance. Due to the differences between PtNiNW catalyst investigated in this work and other alloy nanoparticle or extended surface catalysts, the proper ex situ or in situ processing or ionomer content were not known. Therefore, the goal of this work was to understand the processing and electrode design considerations necessary to obtain an MEA that maximizes the ECA and activity of the catalyst. As such, the experiments reported here were designed to determine the dependence of fuel cell performance on catalyst processing and ionomer content. Through the use of in situ performance testing, advanced in situ diagnostic techniques, and electron microscopy these dependencies were determined, laying a foundation for future development of both the catalyst and the electrode.

Experimental

Nanowire preparation.—PtNiNWs were prepared through spontaneous galvanic displacement (SGD) of nickel nanowires (PlasmaChem GmbH) as described previously.[39] After SGD, the wires were annealed in a hydrogen environment. The samples were heated with a 10°C/minute heating rate to 250°C and then held there for 2 hours. The pressure was maintained at 500 Torr with flowing 300 standard cubic centimeters (sccm) of 50% H_2/50% N_2. The materials obtained are referred to in this paper as as-synthesized.

Ink preparation.—The PtNiNW inks were prepared by weighing PtNiNWs into a glass vial. This was followed by the addition of water (0.2 mL/mg PtNi) and 1-propanol (0.8 mL/mg PtNi). The ink-containing vial was then placed in a beaker filled with ice water, where the mixture was tip sonicated for 2 min (QSonica Misonix S-400, 20 kHz, Amplitude = 1). 20 wt% Nafion solution (D2020, Ion Power) was then added to achieve the desired PtNi:Nafion ratio. The ink was then tip sonicated again for 3 min.

Pt/HSC (TKK TEC10E50E) inks were prepared by weighing the catalyst powder into a glass vial. To which water (0.13 mL/mg Pt/HSC) and 1-propanol (0.1 mL/mg Pt/HSC) were added in that order. The vial was swirled gently after each addition of solvent to ensure all of the catalyst was wet. Next, Nafion solution (D2020, Ion Power) was added (2.11 μL/mg PtHSC). The ink containing vial was then placed in a beaker filled with ice water, where it was then tip sonicated for 10 s. Subsequently, the ink containing vial was sonicated in an ice bath for 20 min. in four increments of 5 min. each with gentle swirling of the vial between increments.

MEA fabrication.—5 cm^2 catalyst-coated membrane electrodes were ultrasonic spray coated (Sonotek Ultrasonic spray system with a 25 kHz Accumist spray head) on to Nafion 212 membranes. Small tabs were sprayed outside the 5 cm^2 area so that the loading and elemental composition of the cathode could be analyzed without influence of the anode. The membrane was held on a porous, heated vacuum plate at 80°C. The inks were sprayed at 0.3 mL/min and a translational speed of 50 mm/s. Multiple passes were used to achieve the desired electrode loadings. The PtNiNW settled very quickly in the inks and it was not possible to spray continuously. Thus after each pass the ink was pulled backed into the syringe and shaken to redisperse the wires. The platinum loading of the cathodes were between 0.1 and 0.2 mg Pt/cm^2. All the MEAs tested in this study contained Pt/HSC anodes with loadings of approximately 0.25 mg Pt/cm^2. After coating the electrode, the hot plate was turned off and the MEAs were allowed to cool before removal from the vacuum plate.

MEA ion exchange.—To probe the impact and reversibility of Ni ion contamination, select MEAs were submerged in 1 L of 0.01 M H_2SO_4 at room temperature for 17 hrs in order to exchange Ni^+ with H^+. After soaking, the MEA was repeatedly rinsed with deionized water and dried on a vacuum plate at 50°C until dry.

XRF analysis.—Loading and elemental compositions were analyzed using a Fischerscope XDV-SDD X-ray fluorescence (XRF) spectrometer with a 50 kV, 50 W X-ray source. Small tabs of electrode material were printed outside the MEA area without the counter electrode on the other side of the membrane. This allowed for elemental analysis of each electrode individually.

Rotating disk electrode.—Half-cell tests were completed using a three-electrode setup. The electrode coating and testing processes were previously optimized for Pt-Ni NWs.[39]

Fuel cell testing.—MEAs were assembled into single test cells using Sigracet SGL 25BC gas diffusion layers (25% compression) and poly(tetrafluoroethylene) gaskets. The active area was 5 cm^2 with single serpentine flow channels. Prior to testing, all the MEAs were preconditioned via voltage cycling using previously published protocols.[43] Electrochemical surface area (ECA) was determined from the hydrogen underpotential deposition (H_{UPD}) region of cyclic voltammograms recorded at 50 mV/s using either a Gamry or Autolab potentiostat. ECA was determined at 30°C, 150 kPa total cell pressure, 100%RH, H_2/N_2 at 0.20/0.05 slpm respectively. Hydrogen-oxygen and hydrogen-air polarization curves were measured at 80°C, 100%RH, 150 kPa_{abs}, and 0.4 slpm. For selected MEAs, after conditioning and performance testing, limiting currents were measured using 200 μm thick teflonated carbon fiber gas diffusion layer possessing a 30 μm microporous layer. The gas diffusion layer was compressed at 15%. A straight pass flow field was used as previously described by Baker et al.[44] Limiting current data was taken at 80°C, 101 kPa total cell pressure, at 75, 60 and 45% RH, under total flows of 1.0/3.144 slpm for the anode and cathode respectively. While the anode gas was pure H_2, the cathode gas was varied to obtain limiting current measurements at 2, 3, 5, 10 and 15 kPa p_{O2}. Due to differences in hardware geometry between the standard and differential cell, the active area for limiting current measurements was 3.24 cm^2.

PtNiNW acid preleaching.—For some MEAs, soluble Ni was leached from the PtNiNWs prior to MEA incorporation (preleaching) by soaking the PtNiNWs in 1 M H_2SO_4 at a concentration of 40 mg PtNi/mL H_2SO_4. The PtNiNWs and H_2SO_4 were added to a 20 mL glass vial. The vial was placed on a roller for the entire leaching processes in an attempt to keep the PtNiNW dispersed and reduce any diffusion limitations. In preliminary experiments to determine the required soaking times to achieve the desired amount of Ni removal it was noticed that lower pH (higher molarity) increased flocculation of the PtNiNWs. To break up the flocs, the vials were periodically removed from the rollers and vigorously shaken. To achieve 81wt% Pt, PtNiNWs were soaked for 2 hours. Leaching for longer than two hours did not remove additional nickel. The mixture was subsequently diluted with deionized water, poured into a centrifuge tube and centrifuged at 2500 rpm for 15 min. The supernatant was poured off and more water was added. This process was repeated two more times. Following centrifugation, the rinsed wires were transferred to glass vials and were dried in a vacuum oven at 110°C and a gauge pressure of −20 inches of Hg. Portions of the wires were annealed after soaking.

Electron microscopy.—Wire morphology and distribution was evaluated by scanning electron microscopy (SEM) using a JEOL

JSM-7000F field emission SEM. Cross-sectional SEM samples were prepared by freezing membranes in liquid nitrogen and cutting across them with a razor. Scanning transmission electron microscopy (STEM) and X-ray energy dispersive spectroscopy (EDS) analysis were obtained using an FEI Talos S/TEM operated at 300 kV and equipped with ChemiSTEM detector.

Results and Discussion

The following sections detail our research to understand the processing steps and electrode composition needed to maximize the performance of PtNiNW catalyst layers. In the As-synthesized and post-leached PtNiNW fuel cell performance section we explore the influence of ionomer content and show the influence of nickel contamination and post-leaching of MEAs to alleviate contamination. In the Pre-leached PtNiNW fuel cell performance section, we use pre-leaching of the PtNiNW catalyst, prior to electrode fabrication, to mitigate Ni contamination. Finally, in the Oxygen transport resistance section we perform limiting current measurements to understand transport mechanisms and limitations in the catalyst layers

As-synthesized and post-leached PtNiNW fuel cell performance.—As-synthesized PtNiNW MEAs were fabricated with varying Nafion contents: 9, 16, and 23 wt% ionomer (relative to total catalyst mass), in order to investigate the role of ionomer content on performance. For comparison, a 50 wt% Pt on high surface area carbon electrode with an ionomer:carbon ratio between 0.8 and 1 (typical for standard PEM fuel cell MEAs) contains approximately 30 wt% ionomer. Lower Nafion contents were initially targeted in this study due to morphological differences of PtNiNWs and their potential to exhibit surface proton conduction. Figure 1 shows SEM images of the cross-section of an MEA along with a top-down image of the PtNiNW cathode. Figure 1 and the subsequent discussion focuses on the 16 wt% Nafion MEA, however other ionomer loadings showed qualitatively similar trends. The cross-sectional image of the MEA in Figure 1a shows that the cathode is approximately 4 μm thick for a 0.13 mg_{Pt}/cm^2 electrode, which is similar to the thickness of Pt/C (50 wt% Pt) of the same loading. The highly porous and contiguous mat of PtNiNWs is readily apparent from the top-down image in Figure 1b. Notably, the diameter and lengths of the PtNiNWs in the MEAs appear unchanged from the as-synthesized PtNiNWs.

The as-synthesized PtNiNW MEAs were assembled into fuel cells for further characterization and were periodically removed from the fuel cell hardware for ion exchange and XRF assessment of Pt/Ni content. Cyclic voltammograms (CVs) were particularly useful for studying the impact of Ni ion contamination on observed properties and performance. Figure 2a shows CVs for a 16 wt% Nafion MEA following a break-in procedure for the as-synthesized MEA and then after two subsequent ion exchanges (as described in the experimental section) after further cell testing. The initial CV lacks classic Pt hydrogen underpotential deposition (H_{upd}) features, indicating an access or reactivity problem characteristic of a 'poisoned' sample. For 3M's NSTF catalyst, it has been observed that the low surface area makes them more susceptible to poisoning than higher surface area catalysts, which is likely the case here, too.[45] In order to remove Ni ions contaminating the ionomer (in electrode and membrane) the MEA was soaked in a dilute sulfuric acid solution (0.01 M) to ion exchange the Ni ions with protons. After the initial ion exchange, the CV shows clear H_{UPD} features with a significant increase in ECA (Figure 2b). From CV features and the measured ECA, the first ion exchange has a significant impact, but the second ion exchange had a much smaller effect. Similar behavior was observed for the 9 wt% and 23 wt% Nafion MEAs.

The elemental composition of the cathode of 16 wt% Nafion MEA as a function of testing and processing steps was measured using X-ray fluorescence spectroscopy (XRF) and is reported in Table I. The as-synthesized MEA was found to have a composition of 14.5 wt% Pt and 84.8 wt% Ni (these PtNiNWs contain a small amount of iron, which is present in the NiNW starting material). Following initial testing, the Ni content decreased significantly from 84.8 (as synthesized) to 57.5 wt%, clearly showing that exposure to cell break-in and operating conditions liberates a substantial portion of Ni from the PtNiNWs. Interestingly, this showed that even before ion exchange that a substantial portion of the Ni is no longer present within the MEA active area. Ion exchanging the MEA further decreased the amount of Ni within the sample, but by a much smaller amount from 57.5 to 54.4 wt%. This corresponds to the removal of 1.75 μmol of Ni. We estimate there are only 0.8 μmol of sulfonic acid sites in the cathode, so this small percentage of Ni is large enough to block every sulfonic acid site, though we cannot say with certainty this was the case.

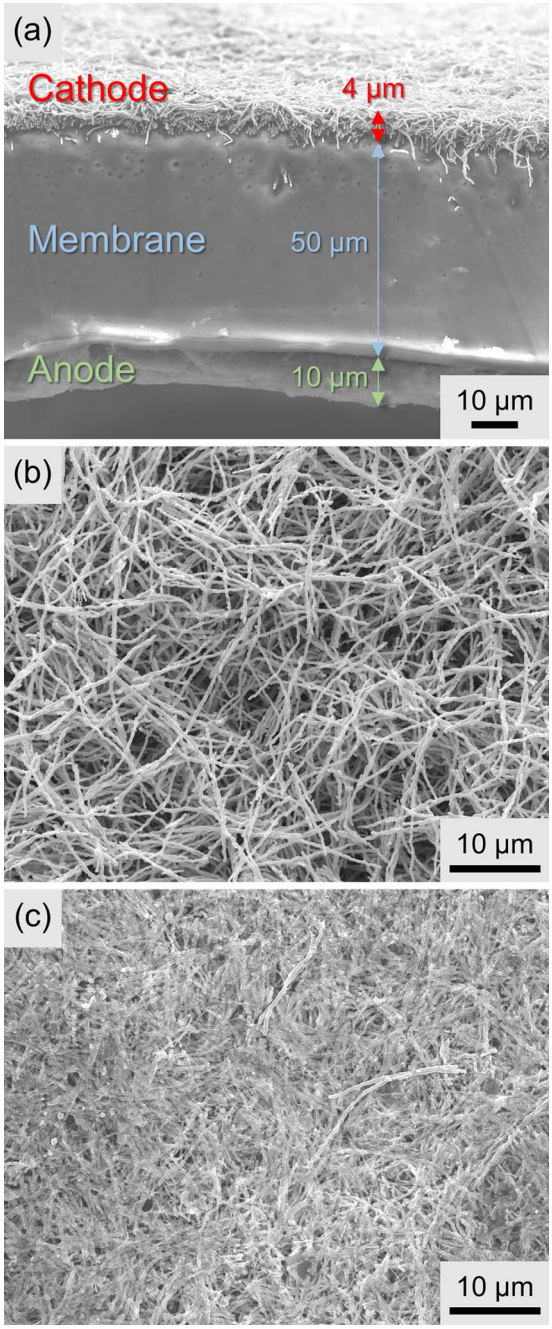

Figure 1. Scanning electron microscope images of the 16 wt% Nafion MEA recorded for the as-prepared MEA in (a) cross-sectional and (b) top-down of the cathode. (c) Top down image of the PtNiNW cathode after performance testing and two ion exchanges. The layer thicknesses reported in (a) are approximate.

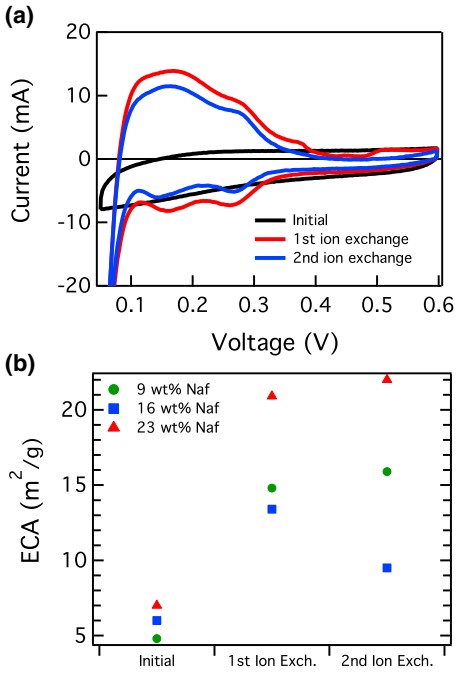

Figure 2. (a) Cycling voltammograms of PtNiNW MEA with 16 wt% Nafion in the cathode. Voltammograms were measured at 50 mV/s after the initial testing cycle and testing cycles following ion exchange in 0.01 M H_2SO_4. (b) Electrochemical surface areas (ECAs) for all of the PtNiNW MEAs.

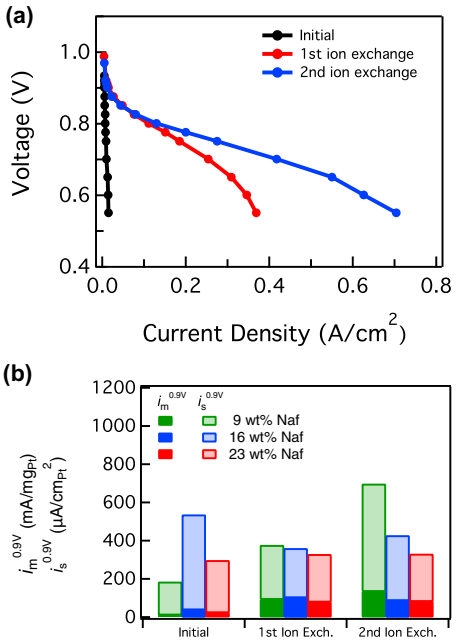

Figure 3. (a) Oxygen polarization curve for the 16 wt% Nafion MEA measured initially and after soaking in 0.01 M H_2SO_4 baths. (b) Mass ($i_m^{0.9\,V}$) and specific ($i_s^{0.9\,V}$) activities measured at 0.9 V for PtNiNW MEAs with 9 wt%, 16 wt%, and 23 wt% Nafion.

Though, this would explain why prior to this ion exchange procedure the PtNiNWs showed no catalytic activity. This fact highlights how little Ni, as a percentage of the starting catalyst material, is required to completely contaminate the cathode. Additional testing and ion exchange steps showed further removal of Ni from the system, but the majority of Ni was removed in the initial testing step. The loss of Ni from the PtNiNWs is also evident in the SEM image of the cathode following testing and ion exchanges as shown in Figure 1c. The PtNiNWs appear to have hollowed and a compaction of the electrode is also apparent.

While CVs and XRF measurements are useful for interpreting observed properties, it is ultimately fuel cell performance that is of primary concern. Figure 3a displays the oxygen polarization curves for the 16 wt% ionomer MEA previously discussed for as-prepared MEAs and after the 1st and 2nd ion exchanges. In the initial testing, the as-prepared cell performance was essentially non-existent, as might have been expected given the lack of electrochemical features observed by CV. This initial behavior of as-prepared MEAs was observed for all ionomer contents studied. (Supporting Information, Fig S1), There is a clear trend of increasing performance after the first and second ion exchanges, which was consistent with CV and XRF data discussed previously. The increase in performance after the first ion exchange can attributed to two main causes. The first is an increase in the ECA of the catalyst, which was shown in the voltammograms in Figure 2, that produced an increase in mass activity of the catalyst. The second is high frequency resistance (HFR). Ion exchanging the MEA reduced the HFR from 480 mΩ-cm^2 during initial testing to 247 mΩ-cm^2 after the first ion exchange. The HFR changes could only account for some of the observed performance losses, and the large overpotential losses are probably most related to catalyst site availability, consistent with other studies of metal ion contamination in fuel cells.[46]

Table I. Weight fraction of Pt and Ni in the cathode of a 16 wt% Nafion MEA measured after different processing and testing steps.

Preceding Process Step	Pt wt%	Ni wt%
As-synthesized	14.5	84.8
Initial Testing	41.5	57.5
1st Ion Exchange	44.3	54.4
2nd Testing	60.3	38.1
2nd Ion Exchange	59.9	38.5
3rd Testing	64.2	34.2

With the second ion exchange there is again an improvement in performance. Consistent with voltammograms, which did not show much change in ECA between the first and second ion exchange, there is only a slight increase in mass activity of the catalyst. Most of the change in the polarization curves between the first and second ion exchanges is in the ohmic and mass-transport regions. The second ion exchange further decreased the HFR to 118 mΩ-cm^2 after the second ion exchange. Also, metal ion contamination has been shown to increase the oxygen transport resistance in the ionomer, which would results in mass-transport losses.[47] Together, the reduction in HFR and oxygen transport resistance would explain the increase in performance following the second ion exchange These results show that Ni contamination effects not only the catalyst but the ionomer in the catalyst layer as well as the membrane.

The mass activity at 0.9 V ($i_m^{0.9\,V}$) and surface area specific activity at 0.9 V ($i_s^{0.9\,V}$) measured as-synthesized and following ion exchange are shown in Figure 3b for all three Nafion-content MEAs tested. After two ion exchanges, there is a general trend of increasing mass and specific activity with decreasing ionomer content, with the 9 wt% Nafion content MEA showing the highest performance on a mass activity basis, 133 mA/mg$_{Pt}$ (0.9 V IR-free). For comparison, PtNi nanoparticles supported on carbon have achieved mass activities over 600 mA/mg$_{Pt}$, so additional refinements in the catalyst processing and electrode design are needed to improve the performance of these PtNiNWs in MEAs. The 9 wt% Nafion MEA had about three times less ionomer (on a mass basis) than a standard Pt/C electrode, suggesting that there may be fundamental difference between the structures of PtNiNW and Pt/C electrodes.

The catalyst performance metrics after two ion exchanges are shown for all three Nafion content MEAs in Table II, along with the RDE-measured values for these PtNiNWs to highlight some of the disparity between MEA and RDE performance.[40] Comparisons

Table II. Electrochemical surface area (ECA), mass activity ($i_m^{0.9\ V}$) and specific activity ($i_s^{0.9\ V}$) for MEAs tested after being two ion exchanges in 0.01 M H_2SO_4 baths. RDE data from Ref. 40.

Nafion wt% Cathode	ECA (m^2/g)	$i_m^{0.9V}$ (mA/mg_{Pt})	$i_s^{0.9V}$ ($\mu A/cm_{Pt}^2$)
RDE	54	1400	2600
9 wt%	19	133	697
16 wt%	21	92	427
23 wt%	25	81	330

between RDE and MEA must be made with caution because the MEA testing conditions are substantially different than the RDE test conditions, however it is still possible to extract meaningful results. The RDE mass activity is about an order of magnitude larger than in an MEA. These differences are much larger that would be observed when comparing RDE and MEA results for Pt/C electrodes, which highlights one of the challenges of developing the catalysts and incorporating them into MEAs. Some of this difference is that the RDE measurements of these PtNiNWs do not suffer from Ni ion contamination in the same way as MEAs, because RDE is run with small catalyst masses and large liquid-electrolyte volumes that maintain Pt accessibility and proton conductivity regardless of Ni dissolution. In RDE, the measured ECA is double that measured in an MEA. In previous RDE measurements we have observed losses in ECA and specific activity associated with Ni loss from ex-situ acid leaching prior to testing, which is due to a dealloying effect.[37] This is consistent with measurements of PtNi NSTF, which have also showed that Ni loss from the core of the material resulted in decreased activity.[9] We have found that PtNiNWs lose less Ni during RDE testing than the MEAs presented here, which may explain some of this large difference. We suspect this difference in Ni loss was due to differences in the electrode coating processes between RDE and MEAs. The MEA catalyst layers were coated using ultrasonic spray. This is a high shear rate process, which may induce some small cracks or fractures that allow for easier access to the Ni core. It is also possible that the mechanical compression of the fuel cell test hardware may strain the materials in a way that made them more susceptible to leaching of Ni. In any case, these results show that even after two ion exchanges of the MEA there is still a large discrepancy between MEA and RDE performances. This led us to investigate a new approach to processing the catalyst.

Pre-leached PtNiNW fuel cell performance.—While it was possible to improve the performance of the as-prepared MEAs with ion exchanges this is time intensive and not feasible in an industrial setting. Therefore, to diminish the potential for Ni contamination the as-prepared catalyst was soaked in 1 M sulfuric acid for 2 hours to leach Ni from the core of the PtNiNW. The goal was not to remove all of the nickel, but the soluble nickel in the core of the PtNiNW that was not alloyed to the Pt. The resulting material had Pt content of 81 wt%, as measured by XRF. The pre-leached PtNiNW powder was analyzed using high-angle annular dark field (HAADF) scanning transmission electron microscopy (STEM). The images in Figure 4a show that the pre-leached wires retained their cylindrical shape but appear to have become hollow tubes with lower mass density in the core. Lower magnification STEM images (not shown) also showed the wires have fractured and are now about 5 μm in length. This was also apparent in SEM of the pre-leached PtNiNW cathode in Figure 4b. Energy-dispersive X-ray spectroscopy (EDS) confirmed that both platinum and nickel were found in the walls of these tubes. This was consistent with our previous studies of acid leaching.[37]

MEAs were prepared with the pre-leached PtNiNWs to determine if the pre-leaching step was sufficient to avoid catastrophic Ni contamination of the ionomer. These MEAs contained 9 wt% Nafion (relative to the mass of pre-leached catalyst) based on the inverse relationship between ionomer content and mass activity observed for the as-prepared PtNiNW MEAs. The cross-sectional SEM of this

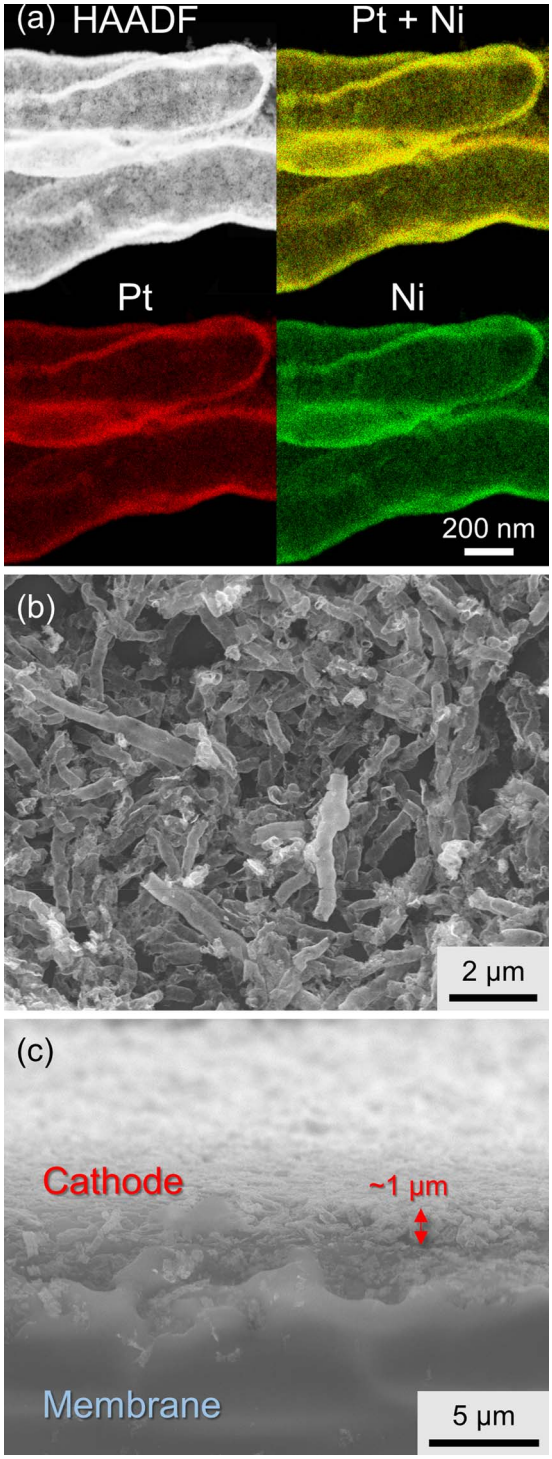

Figure 4. (a) HAADF STEM of 81 wt% Pt PtNiNWs and EDS maps for Pt and Ni, Pt, and Ni. (b) Top-down SEM of the pre leached PtNiNW cathode. (c) Cross-sectional SEM of the pre-leached PtNiNW MEA.

MEA (Figure 4c) showed that this cathode was much thinner (approx. 1 μm) than the as-prepared PtNiNW electrodes (approx. 4 μm), which is consistent with the higher Pt wt% of the pre-leached catalyst.

Like the previously prepared MEAs, the pre-leached PtNiNW MEA was tested before and after ion exchange to assess the impacts of pre-leaching the catalyst and potential Ni contamination. The CV traces and polarization curves from both the initial measurement and after one ion exchange procedure are shown in Figures 5. The initial performance with the pre-leached PtNiNWs was significantly

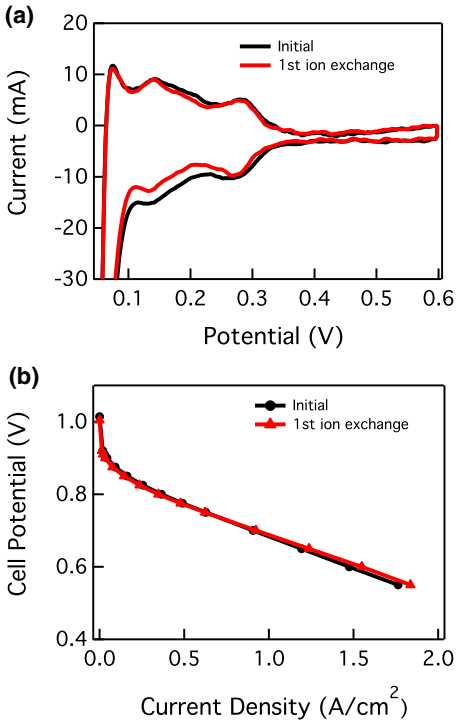

Figure 5. (a) Cyclic voltammograms and (b) oxygen polarization curves of the pre-leached PtNiNW MEA measured without any additional processing of the MEA (initial) and after ion exchanging the MEA in sulfuric acid.

improved compared to the MEAs with as-prepared wires. The initial CV shows the expected H_{UPD} region and the ECA is 22 m^2/g, indicating Ni contamination of the ionomer was not significant in this MEA. XRF measurement confirmed this and showed that that only a small amount of Ni was removed during testing. The initial polarization curve (Figure 5b) showed significantly higher current densities could be achieved in this MEA with the pre-leached PtNiNWs than any of the MEAs with unleached PtNiNWs even after multiple ion exchange processes. The performance metrics from initial testing were a $i_m^{0.9\,V}$ = 238 mA/mg_{Pt} and $i_s^{0.9\,V}$ = 1103 μA/cm_{Pt}^2. The HFR for this MEA was 81 mΩ-cm^2 (at 0.6 V in air), which was lower than any of the as-prepared PtNi MEAs, which measured 118–133 mΩ-cm,^{2} even after they were ion exchanged. This also showed that Ni contamination was not a significant limitation to activity in this MEA. The activity of this MEA is lower than MEAs prepared using PtNi nanoparticles or PtNi NSTF, which have both exceeded the DOE 2020 target of 440 mA/mg_{Pt}.[30,48] However, as mentioned previously, the large-batch synthesis used to prepare these PtNiNWs resulted in lower ORR activity than previous batches prepared in much smaller quantities. Future work on these materials will use materials synthesized through processes that do not exhibit such batch-size dependent losses.[42]

Ion exchanging the MEA by soaking in acid resulted in minor changes in the CV and polarization curves. Unlike the MEAs with unleached PtNiNWs, this ion exchange process did not decrease the HFR of the pre-leached PtNiNW MEA. This provided further confirmation that Ni contamination was not significant with these pre-leached wires and that pre-leaching can be a successful strategy to address Ni ion contamination concerns. Additionally, these results show that MEAs can be fabricated with low ionomer content, which may have benefits for low-loaded MEAs at high current density.

The observed improvements using pre-leached PtNiNWs, still resulted in mass activity far below that found in RDE measurements of these PtNiNWs. With unleached PtNiNWs the best RDE performance was $i_m^{0.9\,V}$ = 1400 mA/mg_{Pt} (ECA = 54 m^2/g, and $i_s^{0.9\,V}$ = 2600 μA/cm_{Pt}^2), as reported in Table II. For a more direct comparison of RDE and MEA properties, the same ink that was used for MEA fabrication was used to fabricate RDE samples. The results from RDE and MEA are compared in Table III. Both have similar ECA, but in RDE measurements the pre-leached PtNiNWs had higher activities than the MEA. This result is not particularly surprising as electrocatalysts in MEAs generally show lower activity than in RDE samples. The difference in ECA between the pre-leached PtNiNWs (MEA and RDE) and the unleached PtNiNWs was also not particularly surprising, as was already noted earlier, previous RDE experiments have shown that leaching Ni reduces surface area.[35,37] It is also possible that differences in ionomer content between the pre-leached and unleached PtNiNW electrodes contributed to this difference. It will be shown shown in the following section that this MEA is not significantly limited by local oxygen-transport at the catalyst surface, thus, this comparison showed that MEA performance was, at least partially limited by the intrinsic properties of the catalyst.

Table III. Comparison of activities and ECA for RDE and MEA samples fabricated from the same ink with pre-leached PtNiNWs.

Sample Type	ECA (m^2/g)	$i_m^{0.9\,V}$ (mA/mg_{Pt})	$i_s^{0.9V}$ (μA/cm_{Pt}^2)
MEA	21	238	1151
RDE	21 ± 1	518 ± 8	2502 ± 49

Oxygen transport resistance.—To better understand the performance of the PtNiNW MEA diffusion-limited current measurements, using methodology described elsewhere, were used to examine the oxygen transport limitations of the atypical PtNiNW electrode structures.[44,49] The measured limiting currents (i_{lim}) were then converted to total electrode transport resistance (R_{Total}) by

$$R_{Total} = \frac{4Fc_{O_2}}{i_{lim}}, \quad [1]$$

where F is the Faraday constant and c_{O2} is the molar concentration of oxygen in the cathode channels. R_{Total} values for the PtNiNW electrodes were compared values for traditional 50 wt% Pt on Vulcan carbon (Pt/Vu) electrodes measured in a separate study.[50] It should be noted that all Pt/Vu electrodes were diluted with Vulcan carbon as to maintain a constant electrode thickness of about 6 μm, which is comparable to the approximately 4 μm thickness of the as-prepared PtNiNW electrode, shown in Figure 1. Figure 6 shows R_{Total} plotted versus inverse Pt roughness factor ($1/f_{Pt}$) for 45, 60, and 75% RH. Limiting current data were measured for 50 wt% Pt/Vu electrodes at nominal loadings of 0.05, 0.075, 0.10 and 0.125 mg_{Pt}/cm^2, where each data point is the average transport resistance of two separate Pt/Vu electrodes with identical loadings. From Figure 6 it was observed that the measured R_{Total} values for Pt/Vu were 1) consistent with those reported elsewhere (see Figure 9 of Reference 49) and 2) increased with decreasing Pt loading. This increase has previously been attributed to an oxygen transport resistance at or near the Pt surface associated with the ionomer.[41,49]

R_{Total} values are also shown for the pre-leached PtNiNW MEA and as-prepared PtNiNW MEAs with 9, 16, and 23 wt% ionomer. These limiting current experiments were performed following performance testing and ion exchanges. It was shown that the PtNiNW MEAs had higher R_{Total} than the Pt/Vu MEAs for all permutations except for the pre-leached PtNiNW MEA at 75%RH. There are several possibilities for this discrepancy that will be discussed below and while they are discussed individually it is possible they are all contributing to R_{Total}.

First, these data in Figure 6 show a general trend of decreased R_{Total} with decreased ionomer content. However, the pre-leached PtNiNW MEA has a lower R_{Total} than the 9 wt% Nafion as-prepared PtNiNW MEA despite the same ionomer content. If instead of considering the ionomer content as a function of total initial catalyst mass it is considered as a function of the mass ratio of Nafion to Pt there is a clear trend in increasing R_{Total} with increasing Nafion content in the electrode, shown in Figure 7. For comparison an optimized Pt/Vu

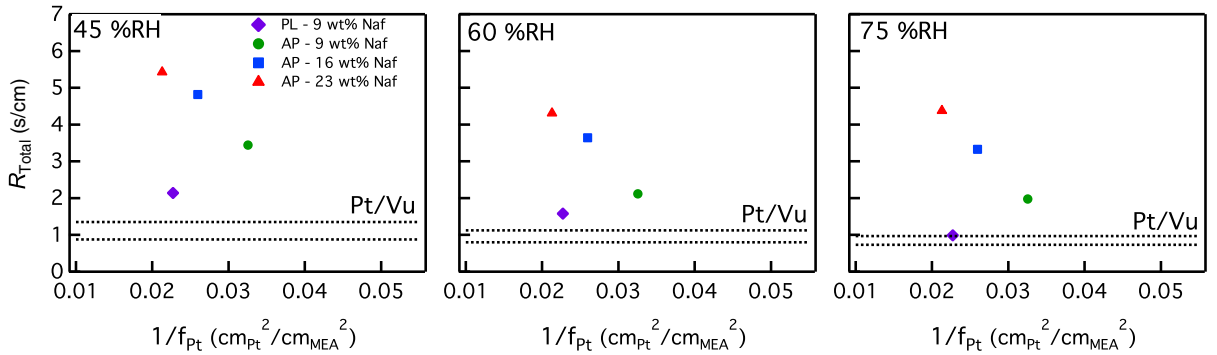

Figure 6. Total electrode transport resistance (R_{Total}) vs inverse Pt roughness factor ($1/f_{Pt}$). R_{Total} values were determined from limiting current measurements at 101 kPa_{abs} cell pressure, 80°C, 2 kPa p_{O2} and 45, 60, or 75%RH. R_{Total} values are shown for 9 wt% Nafion MEA with pre-leached (PL) PtNiNWs and the 9, 16, and 23 wt% ionomer PtNiNW electrodes with as-prepared PtNiNW (AP). These measurements were performed following performance testing and ion exchanges. The dashed lines are the minimum and maximum R_{Total} values for 50 wt% Pt/Vu electrodes measured in a separate study.[50]

(50 wt% Pt, 0.5 ionomer:carbon ratio) is 20 wt% Nafion, yet only at 9 wt% Nafion (pre-leached MEA) is R_{Total} for a PtNiNW electrode the same as the PtVu electrodes. This suggests that ionomer content above 9 wt% is excessive. At this point, we have not explored the role the ionomer content in electrodes with pre-leached PtNiNWs, so additional improvements in performance may be possible with further reductions in ionomer. Considering the nanowire materials have an order of magnitude lower BET surface areas than Pt/Vu it is not surprising that lower ionomer contents on a mass basis result in better performance for the PtNiNW MEAs. With the lower surface area, less ionomer will be needed to create a continuous network for proton transport.

Additionally, the extended surface nature of these materials enables metal-surface proton conduction, which may reduce the amount of ionomer necessary to access catalyst sites.[21] To determine if these mateials also exhibit surface proton conduction, we utilized microstructured scaffolded-electrode (MES) measurements.[51] This unique measurement allows for calculation of the proton conductivity of catalyst materials with or without ionomer binder. Here, the conductivity was measured for PtNiNWs without binder. The conductivity was measured at relative humidities from 45 – 150%RH, as shown in Figure S2a (Supporting Information). As expected, the conductivity increased with increasing RH, until a plateau was reached once the electrode flooded and all of the catalyst surface was able to conduct protons. It was observed that the conductivity plateaued at a lower RH in air than nitrogen due to the local water production from the oxygen reduction reaction increasing the local humidity of the electrode. The observations are consistent with previous MES measurements of ionomer-free Pt black.[52] Our measurements of ionomer-free PtNiNW materials showed equivalent proton conductivity to ionomer-free Pt black (Figure S2b), which is known to exhibit surface proton conduction, indicating these PtNiNWs also exhibit surface proton conduction.[21] Furthermore, the conductivity of the PtNiNWs was equal to ionomer-bound Pt/C suggesting a continuous ionomer network may not be necessary for continuous proton conduction pathways in the catalyst layer. Excess ionomer is likely inhibiting oxygen transport by decreasing electrode pore volume, creating a thicker ionomer coating on the PtNiNW catalyst, or both. For optimized Pt/C electrodes the resistance due to Knudsen diffusion in the pores is small relative to the ionomer resistance, but not enough research has been conducted to know if the same holds for these PtNiNW electrodes.[53]

The second potential cause for increased R_{Total} is that even though an ion exchange process was performed to help rid the PtNiNW MEAs of any contaminating Ni ions, it is possible that some remain, displacing protons inside the ionomer structure and increasing the oxygen transport resistance of the ionomer, which has been observed for cobalt-contaminated membranes and thin films.[47] However, given strong dependence of R_{Total} on ionomer content, shown in Figure 7, it seems like Ni contamination was not the primary influence of R_{Total}. Were Ni contamination the dominate cause of higher R_{Total}, the as-prepared PtNiNW MEAs would have similar R_{Total} regardless of their ionomer content, which is not the case.

The third possibility is that it has been surmised that ionomer confinement on Pt surfaces may be one of the causes for the observed increase in transport resistance at low Pt loadings, a phenomena that may be enhanced on these unsupported, extended surface PtNiNW MEAs.[54,55] However, at this point we do not have enough data on these samples to say whether or not this is the case. In future work we will explore limiting current measurements in greater detail to better

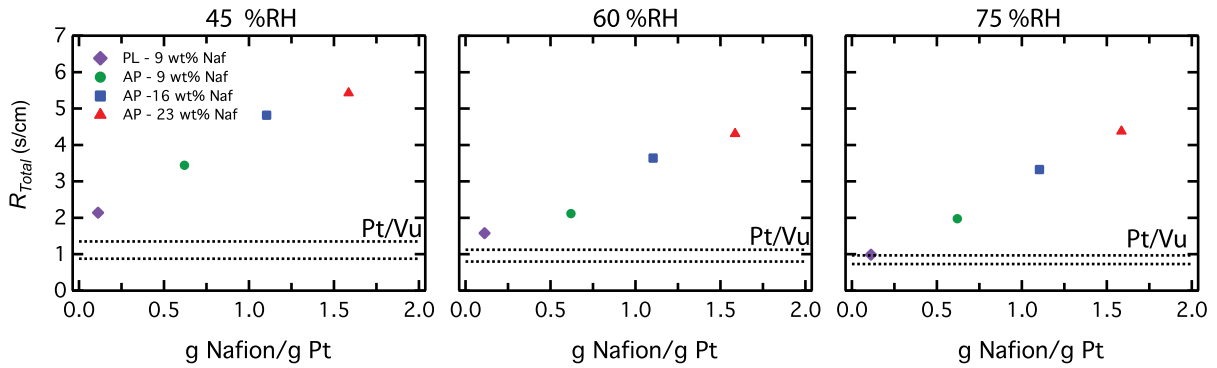

Figure 7. Total electrode transport resistance (R_{Total}) vs Nafion to Pt mass ratio in PtNiNW cathodes measured at 45, 60, and 75%RH. The dashed lines represent the minimum and maximum R_{Total} for Pt/Vu electrodes. R_{Total} values were determined from limiting current measurements at 101 kPa_{abs} cell pressure, 80°C, 2 kPa p_{O2} and 45, 60, or 75%RH.

understand the transport limitations in these MEAs and reduce losses at rated power.

Conclusions

This work demonstrated the challenges associated with fabricating and optimizing PtNiNW MEAs. It was shown that the two keys to maximizing MEA performance were pre-leaching of Ni from the core of the PtNiNW and a low ionomer content to minimize oxygen transport limitations. These results are likely also relevant to other novel electrocatalysts that may have similar electrode optimization concerns. When these two limitations were mitigated, MEA performance was primarily limited by the intrinsic electrochemical characteristics of the catalyst. Future studies will focus on PtNiNWs produced using production methods that produce higher activity catalysts in the large quantities needed for MEA studies. The learnings from this initial study will be applicable to these materials, allowing for easier integration of the materials to MEAs. Furthermore, since these catalyst layers are so thin, the addition of carbon black or other materials to catalyst layer will be explored as means to mitigate potential flooding issues. These studies would not be possible without the initial learnings presented here.

Acknowledgments

This work was supported by the U.S. Department of Energy under Contract No. DE-AC36-08GO28308 with Alliance for Sustainable Energy, LLC, the Manager and Operator of the National Renewable Energy Laboratory. Funding provided by Department of Energy Office of Energy Efficiency and Renewable Energy Fuel Cell Technology Office. The authors would also like to thank Jason Zack for RDE measurements.

ORCID

Scott A. Mauger https://orcid.org/0000-0003-2787-5029
Shaun M. Alia https://orcid.org/0000-0002-7647-9383
Siddharth Komini Babu https://orcid.org/0000-0001-5724-8486
Svitlana Pylypenko https://orcid.org/0000-0001-7982-734X

References

1. T. Soboleva, X. Zhao, K. Malek, Z. Xie, T. Navessin, and S. Holdcroft, *ACS Appl. Mater. Interfaces*, **2**, 375 (2010).
2. J. P. Owejan, J. E. Owejan, and W. Gu, *J. Electrochem. Soc.*, **160**, F824 (2013).
3. S. J. Shin, J. K. Lee, H. Y. Ha, S. A. Hong, and H. S. Chun, *J. Power Sources*, **106**, 146 (2002).
4. C. M. Johnston, K.-S. Lee, T. Rockward, A. Labouriau, N. Mack, and Y. S. Kim, *ECS Trans.*, **25**, 1617 (2009).
5. S. S. Kocha, J. W. Zack, S. M. Alia, K. C. Neyerlin, and B. S. Pivovar, *ECS Trans.*, **50**, 1475 (2013).
6. T. H. Kim, J. Y. Yi, C. Y. Jung, E. Jeong, and S. C. Yi, *Int. J. Hydrog Energy*, **42**, 478 (2017).
7. E. E. Parsonage and M. K. Debe, US Pat. Office, 5,338,430 (1994).
8. M. K. Debe, *U.S. D.O.E. Hydrogen and Fuel Cell Program 2009 Annual Merit Review and Peer Evaluation*, **FC17** (2009).
9. D. A. Stevens, R. Mehrotra, R. J. Sanderson, G. D. Vernstrom, R. T. Atanasoski, M. K. Debe, and J. R. Dahn, *J Electrochem Soc*, **158**, B905 (2011).
10. M. K. Debe, A. J. Steinbach, G. D. Vernstrom, S. M. Hendricks, M. J. Kurkowski, R. T. Atanasoski, P. Kadera, D. A. Stevens, R. J. Sanderson, E. Marvel, and J. R. Dahn, *J. Electrochem. Soc.*, **158**, B910 (2011).
11. L. J. Bregoli, *Electrochimica Acta*, **23**, 489 (1978).
12. B. B. Blizanac, P. N. Ross, and N. M. Markovic, *J. Phys. Chem. B*, **110**, 4735 (2006).
13. S. M. Alia, Y. S. Yan, and B. S. Pivovar, *Catal. Sci. Technol.*, **4**, 3589 (2014).
14. M. K. Debe, A. K. Schmoeckel, G. D. Vernstrom, and R. Atanasoski, *J. Power Sources*, **161**, 1002 (2006).
15. S. Zhang, X.-Z. Yuan, J. N. C. Hin, H. Wang, K. A. Friedrich, and M. Schulze, *J. Power Sources*, **194**, 588 (2009).
16. K. J. J. Mayrhofer, S. J. Ashton, J. C. Meier, G. K. H. Wiberg, M. Hanzlik, and M. Arenz, *J. Power Sources*, **185**, 734 (2008).
17. V. Komanicky, K. C. Chang, A. Menzel, N. M. Markovic, H. You, X. Wang, and D. Myers, *J. Electrochem. Soc.*, **153**, B446 (2006).
18. Y. Shao, J. Wang, R. Kou, M. Engelhard, J. Liu, Y. Wang, and Y. Lin, *Electrochimica Acta*, **54**, 3109 (2009).
19. R. M. Darling and J. P. Meyers, *J. Electrochem. Soc.*, **150**, A1523 (2003).
20. R. Borup, J. Meyers, B. Pivovar, Y. S. Kim, R. Mukundan, N. Garland, D. Myers, M. Wilson, F. Garzon, D. L. Wood III, P. Zelenay, K. L. More, K. Stroh, T. Zawodzinski, J. Boncella, J. E. McGrath, M. Inaba, K. Miyatake et al., *Chem. Rev.*, **107**, 3904 (2007).
21. E. L. Thompson and D. Baker, *ECS Trans.*, **41**, 709 (2011).
22. G. Tamizhmani and G. A. Capuano, *J. Electrochem. Soc.*, **141**, 968 (1994).
23. S. Mukerjee, S. Srinivasan, M. P. Soriaga, and J. McBreen, *J. Electrochem. Soc.*, **142**, 1409 (1995).
24. S. Mukerjee, S. Srinivasan, M. P. Soriaga, and J. McBreen, *J. Phys. Chem.*, **99**, 4577 (1995).
25. U. A. Paulus, A. Wokaun, G. G. Scherer, S. T. J, V. R. Stamenkovic, V. Radmilovic, N. M. Markovic, and P. N. Ross, *J. Phys. Chem. B*, **106**, 4181 (2002).
26. N. Travitsky, T. Ripenbein, and D. Golodnitsky, *J. Power Sources*, **161**, 782 (2006).
27. V. R. Stamenkovic, B. S. Mun, K. J. J. Mayrhofer, P. N. Ross, and N. M. Markovic, *J. Am. Chem. Soc.*, **128**, 8813 (2006).
28. V. R. Stamenkovic, B. S. Mun, M. Arenz, K. J. J. Mayrhofer, C. A. Lucas, G. Wang, P. N. Ross, and N. M. Markovic, *Nat. Mater.*, **6**, 241 (2007).
29. S. Chen, W. Sheng, N. Yabuuchi, P. J. Ferreira, L. F. Allard, and Y. Shao-Horn, *J. Phys. Chem. C*, **113**, 1109 (2009).
30. B. Han, C. E. Carlton, A. Kongkanand, R. S. Kukreja, B. R. Theobald, L. Gan, R. O'Malley, P. Strasser, F. T. Wagner, and Y. Shao-Horn, *Energy Environ. Sci.*, **8**, 258 (2015).
31. Q. Jia, K. Caldwell, K. Strickland, J. M. Ziegelbauer, Z. Liu, Z. Yu, D. E. Ramaker, and S. Mukerjee, *ACS Catalysis*, **5**, 176 (2015).
32. Z. Yu, J. Zhang, Z. Liu, J. M. Ziegelbauer, H. Xin, I. Dutta, D. A. Muller, and F. T. Wagner, *J. Phys. Chem. C*, **116**, 19877 (2012).
33. R. R. Adzic, *U.S. D.O.E. Hydrogen and Fuel Cell Program 2014 Annual Merit Review and Peer Evaluation*, **FC009** (2014).
34. E. Antolini, J. R. C. Salgado, and E. R. Gonzalez, *J. Power Sources*, **160**, 957 (2006).
35. H. R. Colón-Mercado, H. Kim, and B. N. Popov, *Electrochem. Commun.*, **6**, 795 (2004).
36. M. J. Kelly, G. Fafilek, J. O. Besenhard, H. Kronberger, and G. E. Nauer, *J. Power Sources*, **145**, 249 (2005).
37. S. M. Alia, C. Ngo, S. Shulda, M.-A. Ha, A. A. Dameron, J. N. Weker, K. C. Neyerlin, S. S. Kocha, S. Pylypenko, and B. S. Pivovar, *ACS Omega*, **2**, 1408 (2017).
38. A. J. Steinbach, D. van der Vliet, A. E. Hester, J. Erlebacher, C. Duru, I. Davy, M. Kuznia, and D. A. Cullen, *ECS Trans.*, **69**, 291 (2015).
39. S. M. Alia, B. A. Larsen, S. Pylypenko, D. A. Cullen, D. R. Diercks, K. C. Neyerlin, S. S. Kocha, and B. S. Pivovar, *ACS Catalysis*, **4**, 1114 (2014).
40. B. S. Pivovar, *U.S. D.O.E. Hydrogen and Fuel Cell Program 2016 Annual Merit Review and Peer Evaluation*, **FC142** (2016).
41. A. Kongkanand and M. F. Mathias, *J. Phys. Chem. Lett.*, 1127 (2016).
42. B. S. Pivovar, *U.S. D.O.E. Hydrogen and Fuel Cell Program 2017 Annual Merit Review and Peer Evaluation*, **FC142** (2017).
43. P. A. Rapaport, A. J. Blowers, L. James, and B. Lakshmanan, U.S. Pattent Office, 9099703 (2015).
44. D. R. Baker, C. Wieser, K. C. Neyerlin, and M. W. Murphy, *ECS Trans.*, **3**, 989 (2006).
45. R. K. Ahluwalia, J. K. Peng, X. Wang, D. A. Cullen, and A. J. Steinbach, *J. Electrochem. Soc.*, **164**, F306 (2017).
46. T. A. Greszler, T. E. Moylan, and H. A. Gasteiger, in *Handbook of Fuel Cells*, 2nd ed, W. Veilstich, H. A. Gasteiger, A. Lamm, and H. Yokokawa, Editors, p. B631, John Wiley & Sons, Ltd., Chichester, UK (2010).
47. J. Braaten, A. Kongkanand, and S. Litster, *ECS Trans.*, **80**, 283 (2017).
48. A. J. Steinbach, *U.S. D.O.E. Hydrogen and Fuel Cell Program 2017 Annual Merit Review and Peer Evaluation* (2017).
49. T. A. Greszler, D. Caulk, and P. Sinha, *J. Electrochem. Soc.*, **159**, F831 (2012).
50. K. C. Neyerlin, Insights from Electrochemical Diagnostics Pertaining to the Support Dependent Performance of Pt-based Catalysts at High Current Density, *In preparation* (2018).
51. K. C. Hess, W. K. Epting, and S. Litster, *Anal. Chem.*, **83**, 9492 (2011).
52. S. J. An and S. Litster, *ECS Trans.*, **58**, 831 (2013).
53. N. Nonoyama, S. Okazaki, A. Z. Weber, Y. Ikogi, and T. Yoshida, *J. Electrochem. Soc.*, **158**, B416 (2011).
54. A. Kusoglu, D. Kushner, D. K. Paul, K. Karan, M. A. Hickner, and A. Z. Weber, *Adv. Funct. Mater.*, **24**, 4763 (2014).
55. A. Z. Weber and A. Kusoglu, *J. Mater. Chem. A*, **2**, 17207 (2014).